J. Mech. Phys. Solids Vol. 32, No. 1, pp. 63–85, 1984.
Printed in Great Britain.

0022–5096/84 $3.00 + 0.00

PLASTIC FLOW LOCALIZATION DUE TO NON-UNIFORM VOID DISTRIBUTION

N. OHNO

Department of Energy Engineering, Toyohashi University of Technology, Toyohashi, Japan

and

J. W. HUTCHINSON

Division of Applied Sciences, Harvard University, Cambridge, MA 02138, U.S.A.

(*Received* 4 *May* 1983)

ABSTRACT

INFINITE band calculations indicate that the process of flow localization in voided solids is highly sensitive to non-uniformity in void distribution. In this paper, a model is proposed for an elastic–plastic solid with an excess of voids in a disk-shaped cluster embedded in a uniform background distribution. The model is used to study the effect of a void cluster on plastic flow localization. Substantial reductions in ductility due to non-uniformity only occur for quite large clusters when the triaxiality of the overall stresses is low, as in uniaxial tension. At higher stress triaxialities, a small cluster can be severely deleterious.

1. INTRODUCTION

TWO TYPES of calculations have been performed to predict the relation between ductility and hole growth in rate-independent elastic–plastic solids. TVERGAARD's (1981) calculations for a doubly-periodic array of cylindrical voids subject to plane strain deformation represents one type. In the first stage of deformation, the solution is doubly-periodic with the same deformation of the void in each unit cell. Overall ductility terminates when flow localizes along some line of voids. This localization is manifest in the form of loss of uniqueness of the doubly-periodic solution by bifurcation into a banded deformation field.

In the second class of calculations, a continuum constitutive model for a voided, dilating material, such as that proposed by GURSON (1975, 1977), is invoked which specifies a yield condition, a flow law and an evolutionary rule for the volume fraction of voids. Studies, such as those of YAMAMOTO (1978) and SAJE, PAN and NEEDLEMAN (1982), have considered the localization of plastic flow in an infinite block of the material which contains an infinite planar band with an excess void level. The properties within the band are uniform but different from the uniform properties of the material outside the band, so that the entire block of material is characterized by only two states of deformation. The analysis follows the evolution of the difference between these two states. The limit of overall ductility occurs when plastic flow comes to a halt outside the band.

To set the stage for the present study we display in Fig. 1 ductility predictions based on the infinite band calculations of the type reported by YAMAMOTO (1978) and SAJE *et al.* (1982) based on the Gurson model, which will be specified in the next section. For the purpose of the present discussion, the band is restricted to be normal to the z-direction, the principal direction of straining. In Fig. 1(a), the initial void volume fraction outside the band is $f_1 = 0.01$, while the initial value inside the band is denoted by f_1^b. The infinite block is subject to proportional axisymmetric remote stressing such that $\sigma_r^\infty = \sigma_\theta^\infty = \rho\sigma_z^\infty$ where ρ is held fixed. The ductility limit, $(\varepsilon_z^\infty)_{cr}$, is associated with the maximum strain attained outside the band, as described above. Curves of ductility versus the initial volume fraction difference, $\Delta \equiv f_1^b - f_1$, are shown in Fig. 1(a) for three levels of overall stress triaxiality as measured by ρ. This figure brings out the exceptionally strong dependence of ductility on remote stress triaxiality and non-uniformity in the initial void volume fraction. The material is highly imperfection-sensitive to non-uniformity in initial void distribution—so much so, that the *slope* of the relation between $(\varepsilon_z^\infty)_{cr}$ and Δ becomes infinite as $\Delta \to 0$, as can be seen in Fig. 1(a). In the limit problem for $\Delta = 0$, localization appears at $(\varepsilon_z^\infty)_{cr}$ in the form of a bifurcation solution having continuing deformation in the band and no additional plastic deformation outside it (RICE, 1976).

The strong sensitivity of ductility to non-uniformity in void distribution is brought out even more clearly in Fig. 1(b) where ductility curves for constant ratios of f_1 to f_1^b are plotted against f_1^b, in each case for $\rho = 0.25$. Only a 5% difference between f_1 and f_1^b results in a factor of about two reduction of ductility below that for the material with a uniform distribution.

Predictions from the infinite band model provide the only available theoretical insight into the effect of non-uniformity in void distributions on ductility. Realistic void distributions are, in general, inherently three-dimensional and calculations based on them have not yet been attempted. In this paper we make a first attempt to gain some insight into the effect the *size* of the region of non-uniformity has on variations in ductility. The model we will introduce allows for a spatial distribution of voids in a band as depicted in Fig. 2. Details of the model will be spelled out later. Here, however, we simply note that Gurson theory will be used to characterize the material, and the initial void volume fraction within the band will be taken to be axisymmetric with

$$f_1^b = f_1 + \Delta \exp\left\{-\frac{1}{2}\left(\frac{r}{s\lambda}\right)^2\right\}. \tag{1}$$

The initial thickness of the band λ enters the analysis as an arbitrary scale length, which will be identified with the initial average void spacing when we interpret results. Other conventions are shown in Fig. 2. The initial void volume fraction outside the band is uniform and given by f_1, and this same value is approached inside the band for $r \gg s\lambda$. Thus, the non-uniformity of the initial void distribution is a disk-shaped cluster of thickness λ and approximate radius $s\lambda$ whose excess in volume fraction at its center over the uniform background level is Δ.

The model is formulated to permit contact with the results based on a uniform distribution within the band (hereafter referred to as the uniform band results). For a given Δ, the uniform band results will be obtained when $s \to \infty$, while the bifurcation limit corresponding to a uniform distribution with $f = f_1$ will be obtained as $s \to 0$. Our

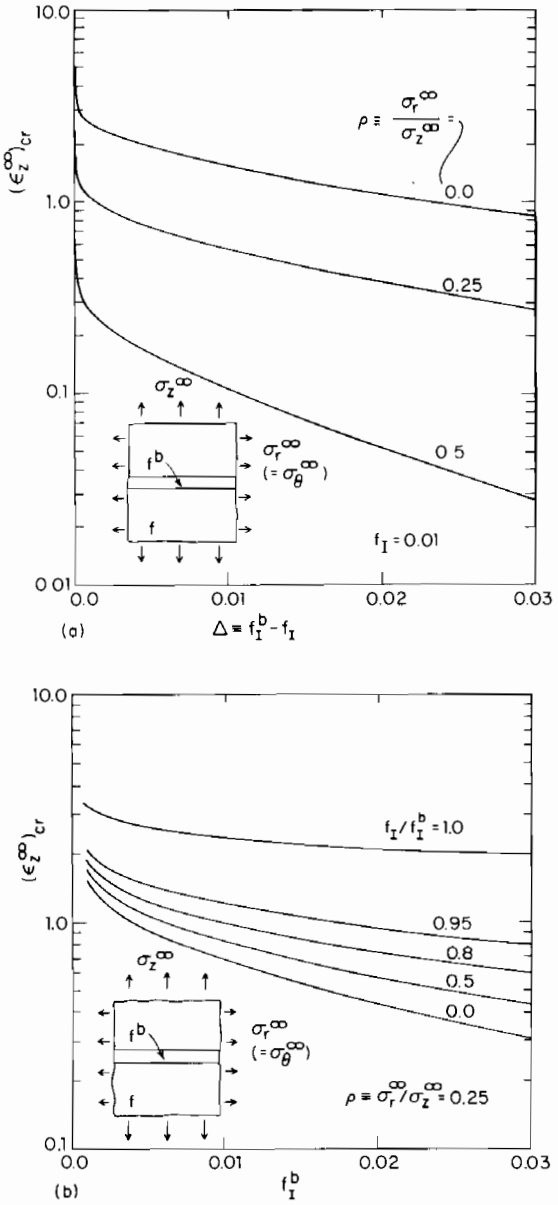

FIG. 1. Critical strain for the onset of plastic flow localization in an infinite band perpendicular to the direction of maximum principal stress σ_z^∞ ($\nu = 0.3$, $\varepsilon_y = 0.0033$ and $N = 0.1$). (a) Ductility vs initial void volume fraction difference for various stress triaxialities ($f_I = 0.01$ in all cases). (b) Ductility vs initial void volume fraction in band for various ratios of f_I/f_I^b ($\rho = 0.25$ in all cases).

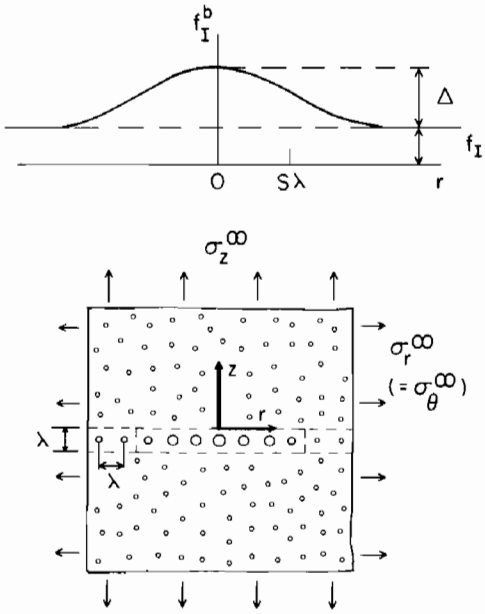

FIG. 2. Conventions.

main aim is to determine the effect of cluster size as measured by s on the ductility. In particular, we seek to discover how large s must be such that the uniform band results become applicable. It will be seen that the answer to this latter question depends strongly on the triaxiality level ρ.

2. GURSON MODEL FOR A VOIDED, RATE-INDEPENDENT SOLID

The Gurson model (1975, 1977) has been formulated to incorporate void nucleation as well as void growth. While nucleation is undoubtedly an important factor in the effects of non-uniformities, we shall confine our attention here to voids which are initially present at zero strain. The equations of the Gurson model have been used by a number of authors and therefore we will summarize these equations as briefly as possible in the form to be used here. TVERGAARD (1981, 1982a) has suggested a slight modification of these equations which will be adopted.

The current overall stress and void volume fractions are denoted by σ_{ij} and f. Cartesian components will be used and the stress components are those of the Cauchy true stress. The matrix material itself (or equivalently the material with $f = 0$) is assumed to be characterized by a uniaxial true stress–logarithmic strain relation of the form

$$\bar{\sigma}/\sigma_y = \begin{cases} \bar{\varepsilon}/\varepsilon_y, & \bar{\varepsilon} \leqslant \varepsilon_y, \\ (\bar{\varepsilon}/\varepsilon_y)^N, & \bar{\varepsilon} > \varepsilon_y, \end{cases} \tag{2}$$

where σ_y is the yield stress, $\varepsilon_y = \sigma_y/E$ is the yield strain and E is Young's modulus.

Given the current level of effective flow stress $\bar{\sigma}$ in the matrix material, the yield condition for the voided material in terms of the overall stress σ_{ij} is

$$\Phi(\sigma_e, \sigma_{kk}) = \left(\frac{\sigma_e}{\bar{\sigma}}\right)^2 + 2fq_1 \cosh\left(\tfrac{1}{2}q_2\sigma_{kk}/\bar{\sigma}\right) - (1+q_3 f^2) = 0, \tag{3}$$

where $\sigma_e = (3\sigma'_{ij}\sigma'_{ij}/2)^{1/2}$ is the effective stress and σ'_{ij} is the stress deviator. Following the recommendation of Tvergaard, $q_1 = 3/2$, $q_2 = 1$ and $q_3 = q_1^2$. The overall inelastic strain-rate is denoted by $\dot{\varepsilon}^{\mathrm{p}}_{ij}$ and the rate of change of the void volume fraction is related to it by

$$\dot{f} = (1-f)\dot{\varepsilon}^{\mathrm{p}}_{kk}. \tag{4}$$

The condition, $\sigma_{ij}\dot{\varepsilon}^{\mathrm{p}}_{ij} = (1-f)\bar{\sigma}\dot{\bar{\varepsilon}}^{\mathrm{p}}$, equating the overall plastic work rate to the matrix plastic work rate per unit volume leads to the evolutionary equation for $\bar{\sigma}$

$$\dot{\bar{\sigma}} = h[(1-f)\bar{\sigma}]^{-1}\sigma_{ij}\dot{\varepsilon}^{\mathrm{p}}_{ij}, \tag{5}$$

where

$$\frac{1}{h} \equiv \frac{\mathrm{d}\bar{\varepsilon}^{\mathrm{p}}}{\mathrm{d}\bar{\sigma}} = \frac{1}{E}\left[\frac{1}{N}\left(\frac{\bar{\sigma}}{\sigma_y}\right)^{(1-N)/N} - 1\right] \quad \text{for } \bar{\sigma} \geqslant \sigma_y. \tag{6}$$

Normality of inelastic flow to the yield surface gives the flow law for continued plastic loading

$$\dot{\varepsilon}^{\mathrm{p}}_{ij} = \frac{1}{H}\left(\frac{\bar{\sigma}}{2}\right)^2 \frac{\partial\Phi}{\partial\sigma_{ij}} \frac{\partial\Phi}{\partial\sigma_{kl}} \overset{\nabla}{\sigma}_{kl}, \tag{7}$$

where

$$\frac{\bar{\sigma}}{2}\frac{\partial\Phi}{\partial\sigma_{ij}} = \frac{3}{2}\frac{\sigma'_{ij}}{\bar{\sigma}} + \alpha\delta_{ij}, \tag{8}$$

$$\alpha = \tfrac{1}{2}q_1 q_2 f \sinh\left(\tfrac{1}{2}q_2\frac{\sigma_{kk}}{\bar{\sigma}}\right), \tag{9}$$

$$H = \frac{\bar{h}}{1-f}\left[\left(\frac{\sigma_e}{\bar{\sigma}}\right)^2 + \alpha\frac{\sigma_{kk}}{\bar{\sigma}}\right]^2 - 3\bar{\sigma}(1-f)\alpha\left[q_1 \cosh\left(\frac{q_2}{2}\frac{\sigma_{kk}}{\bar{\sigma}}\right) - q_3 f\right] \tag{10}$$

and δ_{ij} is the Kronecker delta. The spin-invariant Jaumann stress-rate $\overset{\nabla}{\sigma}_{ij}$ is used in (7).

The reduction in the elastic moduli due to the presence of the voids is neglected and the elastic part of the strain-rate is taken to be given by

$$\dot{\varepsilon}^{\mathrm{e}}_{ij} = \frac{1+\nu}{E}\overset{\nabla}{\sigma}_{ij} - \frac{\nu}{E}\overset{\nabla}{\sigma}_{kk}\delta_{ij}, \tag{11}$$

where ν is Poisson's ratio. The rate constitutive relation can be inverted to give

$$\overset{\nabla}{\sigma}_{ij} = L_{ijkl}\dot{\varepsilon}_{kl}, \tag{12}$$

where

$$L_{ijkl} = L^{\mathrm{e}}_{ijkl} - \frac{(G\sigma'_{ij}/\bar{\sigma} + K\alpha\delta_{ij})(G\sigma'_{kl}/\bar{\sigma} + K\alpha\delta_{kl})}{(1/9)H + (G/3)(\sigma_e/\bar{\sigma})^2 + K\alpha^2}, \tag{13}$$

$$L^e_{ijkl} = G(\delta_{ik}\delta_{jl}+\delta_{il}\delta_{jk})+(K-\tfrac{2}{3}G)\delta_{ij}\delta_{kl}, \tag{14}$$

with $G = E/[2(1+\nu)]$ and $K = E/[3(1-2\nu)]$. For an elastic increment, i.e. for

$$\Phi < 0, \quad \text{or} \quad \Phi = 0 \quad \text{and} \quad \frac{1}{H}\frac{\partial \Phi}{\partial \sigma_{ij}}\overset{\nabla}{\sigma}_{ij} < 0, \tag{15}$$

the moduli are taken to be $\mathbf{L}^e$.

It will be useful to cast the rate equations in terms of the updated nominal stress-rate, which is related to the Jaumann rate by

$$\dot{n}_{ij} = \overset{\nabla}{\sigma}_{ij} - \sigma_{ik}\Omega_{kj} - \dot{\varepsilon}_{ik}\sigma_{kj} + \dot{\varepsilon}_{kk}\sigma_{ij}. \tag{16}$$

Here, Ω_{ij} is the spin tensor so that with $\dot{u}_i$ as the displacement-rate and with $(\,)_{,i} = \partial(\,)/\partial x_i$,

$$\dot{\varepsilon}_{ij} = \tfrac{1}{2}(\dot{u}_{i,j}+\dot{u}_{j,i}) \quad \text{and} \quad \Omega_{ij} = \tfrac{1}{2}(\dot{u}_{i,j}-\dot{u}_{j,i}). \tag{17}$$

In our model of the axisymmetric band undergoing axisymmetric deformations, rotation is not expected to play an important role. In formulating the model we will neglect any rotation of the interface between the band and the semi-infinite half-space when we apply continuity conditions across the interface. For consistency and convenience, we also neglect the spin term $\sigma_{ik}\Omega_{kj}$ in (16). With this spin term neglected, the rate-constitutive relation can be recast as

$$\dot{n}_{ij} = c_{ijkl}\dot{\varepsilon}_{kl}, \tag{18}$$

where

$$c_{ijkl} = L_{ijkl} - \tfrac{1}{2}\delta_{ik}\sigma_{jl} - \tfrac{1}{2}\delta_{il}\sigma_{jk} + \sigma_{ij}\delta_{kl}. \tag{19}$$

3. Model for Analyzing Localization in Presence of a Disk-shaped Cluster of Excess Voids

3.1. *Description of model*

The material is everywhere characterized by Gurson theory. Attention is restricted to initial void distributions which are axisymmetric with respect to the z-axis and to subsequent deformations which preserve this axial symmetry. At triaxiality levels as low as $\rho = 0$ (uniaxial tension) the critical orientation of a localization band is likely to be inclined to the axis of principal strain. However at somewhat higher triaxialities, axisymmetric localization bands are commonly observed as the center section of the cup-cone fracture of a round tensile bar. As depicted in Fig. 2, an infinite planar band of initial thickness λ contains a non-uniform distribution of initial void volume fraction $f_1^b(r)$ given by equation (1). Everywhere outside the band the initial void volume fraction is the uniform value f_1, which also corresponds to the limit in the band for large r. Proportional, remote axisymmetric stressing will be prescribed such that $\sigma_r^\infty = \sigma_\theta^\infty = \rho\sigma_z^\infty$ with ρ fixed.

The initial thickness of the band λ enters the analysis as a scale length that can be prescribed arbitrarily. The initial void distribution in the band (1) is also scaled by λ.

The essence of localization once it is underway is the accelerated growth of a single plane of voids. Thus, in interpreting the results from the model, we will identify λ with the initial average void spacing, as depicted in Fig. 2. Application of a continuum theory such as the Gurson model is usually restricted to characteristic deformation wavelengths which are large compared to the average void spacing. However, the stress–strain relation of the Gurson model was obtained from the approximate analysis of a unit voided cell whose size was identified with the void spacing. Thus it is not inappropriate to use the Gurson theory to characterize the material in the band even when λ is identified with the initial average void spacing.

In principle, a numerical method such as the finite element method could be used to solve the governing equations and follow the evolution of the void volume fraction throughout the body. We have elected to make some further simplifications to the model so as to make it more amenable to analysis. First, rotation and shearing in the band will be neglected. This approximation is justified as long as the in-plane dimension of the cluster is large compared to λ, i.e. $s > 1$. The non-zero strain-rates in the band ($\dot{\varepsilon}_r$, $\dot{\varepsilon}_\theta$ and $\dot{\varepsilon}_z$) will be taken to be independent of z. A second important simplification is that spatial variations of the incremental moduli outside the band will be ignored. At each instant in the deformation history, the incremental moduli in the material outside the band will be taken to be the incremental moduli associated with the remote stress state $\boldsymbol{\sigma}^\infty$. Furthermore, as already mentioned, rotation of the interface will be ignored in applying conditions of continuity of traction-rates and displacement-rates between the band and the half-spaces outside the band.

3.2. *Governing equations, reduction to an integral equation, and critical condition for localization*

At a given instant in the deformation history the non-zero components of the nominal stress-rate and strain-rate in the band are related by

$$\begin{pmatrix} \dot{n}_r^b \\ \dot{n}_\theta^b \\ \dot{n}_z^b \end{pmatrix} = \begin{pmatrix} L_{11}^b & L_{12}^b+\sigma_r^b & L_{13}^b+\sigma_r^b \\ L_{12}^b+\sigma_\theta^b & L_{22}^b & L_{23}^b+\sigma_\theta^b \\ L_{13}^b+\sigma_z^b & L_{23}+\sigma_z^b & L_{33}^b \end{pmatrix} \begin{pmatrix} \dot{\varepsilon}_r^b \\ \dot{\varepsilon}_\theta^b \\ \dot{\varepsilon}_z^b \end{pmatrix}, \tag{20}$$

where $L_{ij}^b = L_{iijj}^b$ (no sum). The incremental moduli in the band are functions of r due to their dependence on the initial void volume fraction $f_1^b(r)$ and due to the r-dependence which stresses in the band, $\boldsymbol{\sigma}^b(r)$, develop.

Outside the band, from (18),

$$\dot{n}_{ij} = c_{ijkl}^\infty \dot{\varepsilon}_{kl}, \tag{21}$$

where the $\mathbf{c}^\infty$ are evaluated at infinite. For the region outside the band, denote all quantities associated with conditions at infinite by a superscript $(\,)^\infty$ and let

$$\dot{n}_{ij} = \dot{n}_{ij}^\infty + \dot{n}_{ij}^*, \quad \dot{u}_{i,j} = \dot{u}_{i,j}^\infty + \dot{u}_{i,j}^*, \quad \dot{\varepsilon}_{ij} = \dot{\varepsilon}_{ij}^\infty + \dot{\varepsilon}_{ij}^*, \tag{22}$$

where the additional parts are denoted by $(\,)^*$ and they satisfy

$$(\dot{n}_{ij}^*, \dot{\varepsilon}_{ij}^*, \dot{u}_{i,j}^*) \to 0 \quad \text{as} \quad r^2+z^2 \to \infty. \tag{23}$$

Then, (21) can be split according to

$$\dot{n}_{ij}^{\infty} = c_{ijkl}^{\infty}\dot{\epsilon}_{kl}^{\infty} \quad \text{and} \quad \dot{n}_{ij}^{*} = c_{ijkl}^{\infty}\dot{\epsilon}_{kl}^{*} \tag{24}$$

or, because of the transverse isotropy with respect to the z-axis, as

$$\begin{pmatrix} \dot{n}_r^{\infty} \\ \dot{n}_z^{\infty} \end{pmatrix} = \begin{pmatrix} L_{11}^{\infty} + L_{12}^{\infty} + \sigma_r^{\infty} & L_{13}^{\infty} + \sigma_r^{\infty} \\ 2(L_{13}^{\infty} + \sigma_z^{\infty}) & L_{33}^{\infty} \end{pmatrix} \begin{pmatrix} \dot{\epsilon}_r^{\infty} \\ \dot{\epsilon}_z^{\infty} \end{pmatrix}, \tag{25}$$

$$\begin{pmatrix} \dot{n}_r^{*} \\ \dot{n}_\theta^{*} \\ \dot{n}_z^{*} \end{pmatrix} = \begin{pmatrix} L_{11}^{\infty} & L_{12}^{\infty} + \sigma_r^{\infty} & L_{13}^{\infty} + \sigma_r^{\infty} \\ L_{12}^{\infty} + \sigma_r^{\infty} & L_{11}^{\infty} & L_{13}^{\infty} + \sigma_r^{\infty} \\ L_{13}^{\infty} + \sigma_z^{\infty} & L_{13}^{\infty} + \sigma_z^{\infty} & L_{33}^{\infty} \end{pmatrix} \begin{pmatrix} \dot{u}_{r,r}^{*} \\ \dot{u}_r^{*}/r \\ \dot{u}_{z,z}^{*} \end{pmatrix}, \tag{26}$$

$$\left.\begin{aligned} \dot{n}_{rz}^{*} &= (L_{44}^{\infty} - \tfrac{1}{2}\sigma_z^{\infty})(\dot{u}_{r,z}^{*} + \dot{u}_{z,r}^{*}), \\ \dot{n}_{zr}^{*} &= (L_{44}^{\infty} - \tfrac{1}{2}\sigma_r^{\infty})(\dot{u}_{r,z}^{*} + \dot{u}_{z,r}^{*}), \end{aligned}\right\} \tag{27}$$

where $L_{ij}^{\infty} = L_{iijj}^{\infty}$ (no sum) and $L_{44}^{\infty} \equiv L_{1313}^{\infty} = L_{1212}^{\infty}$. Our neglect of the spin term $\boldsymbol{\sigma\Omega}$ in arriving at (18) has no effect on equations (20), (25) and (26). Only (27) is affected by having omitted this term. The omission has essentially no influence since L_{44}^{∞} is the elastic shear modulus G during the entire history and coefficients proportional to the stresses which were neglected in arriving at (27) are, by comparison, very small.

Since $\dot{\mathbf{n}}^{\infty}$ is uniform, incremental equilibrium requires

$$\dot{n}_{r,r}^{*} + (\dot{n}_r^{*} - \dot{n}_\theta^{*})/r + \dot{n}_{zr,z}^{*} = 0, \tag{28}$$

$$\dot{n}_{z,z}^{*} + \dot{n}_{rz,r}^{*} + \dot{n}_{rz}^{*}/r = 0. \tag{29}$$

Because of symmetry with respect to the central plane of the band, only the upper half-space need be considered. Continuity of traction-rates and displacement-rates across the interface between the band and the upper-half space is met if

$$\dot{n}_z^{\mathrm{b}}(r) = \dot{n}_z^{\infty} + \dot{n}_z^{*}(r, 0), \tag{30}$$

$$\dot{n}_{zr}^{\mathrm{b}}(r) = \dot{n}_{zr}^{*}(r, 0) = 0, \tag{31}$$

$$\dot{u}_r^{\mathrm{b}}(r) = r\dot{\epsilon}_r^{\infty} + \dot{u}_r^{*}(r, 0) \quad (\text{or } \dot{\epsilon}_r^{\mathrm{b}}(r) = \dot{\epsilon}_r^{\infty} + \dot{\epsilon}_r^{*}(r, 0)) \tag{32}$$

and

$$\dot{\epsilon}_z^{\mathrm{b}}(r)\lambda \exp\{\epsilon_z^{\mathrm{b}}(r)\} = \dot{\epsilon}_z^{\infty}\lambda \exp\{\epsilon_z^{\infty}\} + 2\dot{u}_z^{*}(r, 0). \tag{33}$$

In words, (33) states that the rate of thickness increase at any point in the band over the corresponding rate at infinity must equal the additional separation-rate $2\dot{u}_z^{*}(r, 0)$ of the faces of the half-space. As previously mentioned, we have taken the current normal to the half-space to be in the z-direction, consistent with the assumption of small rotations. Furthermore, rate quantities on the interface in the material outside the band are evaluated at the same z-value, which for convenience has been taken to be $z = 0$.

Substitution of $(20)_3$, $(25)_2$, (32), and (33) into (30) results in

$$\dot{n}_z^{*}(r, 0) - (L_{13}^{\mathrm{b}} + \sigma_z^{\mathrm{b}})\frac{\partial \dot{u}_r^{*}(r, 0)}{\partial r} - (L_{23}^{\mathrm{b}} + \sigma_z^{\mathrm{b}})\frac{\dot{u}_r^{*}(r, 0)}{r} - L_{33}^{\mathrm{b}}\frac{2\dot{u}_z^{*}(r, 0)}{\lambda \exp(\epsilon_z^{\mathrm{b}})} = \dot{q}(r), \tag{34}$$

where

$$\dot{q}(r) = [L_{13}^{\mathrm{b}} + L_{23}^{\mathrm{b}} - 2L_{13}^{\infty} + 2(\sigma_z^{\mathrm{b}} - \sigma_z^{\infty})]\dot{\epsilon}_r^{\infty} + [\exp(\epsilon_z^{\infty} - \epsilon_z^{\mathrm{b}})L_{33}^{\mathrm{b}} - L_{33}^{\infty}]\dot{\epsilon}_z^{\infty}. \tag{35}$$

Thus, the boundary conditions have been reduced to (34) and to (31) or, by (27), to

$$\dot{u}^*_{r,z} + \dot{u}^*_{z,r} = 0. \tag{36}$$

The semi-infinite half-space above the band has uniform moduli with transverse isotropy with respect to the z-axis. Since the loading is axisymmetric, the solution also preserves axial symmetry. A general representation of the solution to the incremental field equations in this upper-half space can be obtained along the lines first indicated by ELLIOTT (1948, 1949), as discussed further in the Appendix. The general solution for the starred quantities which meets the boundary condition (36) gives

$$\dot{u}^*_r(r,0) = -\int_0^\infty \alpha_1 g(\xi)\xi^2 J_1(\xi r)\,\mathrm{d}\xi, \tag{37}$$

$$\dot{u}^*_z(r,0) = -\int_0^\infty \alpha_2 g(\xi)\xi^2 J_0(\xi r)\,\mathrm{d}\xi, \tag{38}$$

$$\dot{n}^*_z(r,0) = \int_0^\infty \alpha_3 g(\xi)\xi^3 J_0(\xi r)\,\mathrm{d}\xi. \tag{39}$$

Here $g(\xi)$ is an unknown function which will be chosen to meet the other boundary condition (34), and J_0 and J_1 are Bessel functions of the first kind of order zero and one, respectively. In addition,

$$\alpha_1 = 1 - \frac{\bar{\mu}^{1/2}}{\mu^{1/2}}\frac{1+k}{1+\bar{k}}, \quad \alpha_2 = \frac{1}{\mu^{1/2}}\frac{k-\bar{k}}{1+\bar{k}},$$
$$\alpha_3 = \frac{k}{\mu}L^\infty_{33} - L^\infty_{13} - \sigma^\infty_z - \frac{\bar{\mu}^{1/2}}{\mu^{1/2}}\frac{1+k}{1+\bar{k}}\left(\frac{\bar{k}}{\bar{\mu}}L^\infty_{33} - L^\infty_{13} - \sigma^\infty_z\right), \tag{40}$$

where μ, $\bar{\mu}$, k and $\bar{k}$ are functions of $\mathbf{L}^\infty$ and $\boldsymbol{\sigma}^\infty$ given in the Appendix.

The function $g(\xi)$ is determined by substituting (37)–(39) into (34):

$$\int_0^\infty K(\xi, r)g(\xi)\,\mathrm{d}\xi = \dot{q}(r), \tag{41}$$

where

$$K(\xi,r) = [\alpha_3 + \alpha_1(L^b_{13} + \sigma^b_z)]\xi^3 J_0(\xi r) - \alpha_1(L^b_{13} - L^b_{23})r^{-1}\xi^2 J_1(\xi r) + 2\alpha_2 L^b_{33}[\lambda \exp(\varepsilon^b_z)]^{-1}\xi^2 J_0(\xi r). \tag{42}$$

It is recalled that quantities labeled with a superscript b are associated with the solution in the band and are functions of r. The loading term, $\dot{q}(r)$, in (41) which is given by (35) depends on the current state and on the remotely specified strain increments $\dot{\boldsymbol{\varepsilon}}^\infty$. Solution of the integral equation (41) for $g(\xi)$ provides the entire solution to the incremental boundary value problem, since incremental quantities in the band can then be obtained from the interface equations (30)–(33) together with (20). Thus, if the history of remote stress or strain is specified, the behavior in the band, including the evolving void distribution $f^b(r)$, can be obtained by the solution of a sequence of incremental boundary value problems governed by (41).

As remote straining increases, an eigenstate is reached where the integral equation

(41) admits a non-zero, homogeneous solution, i.e. a non-trivial solution exists to

$$\int_0^\infty K(\xi, r)g(\xi)\,\mathrm{d}\xi = 0. \tag{43}$$

When this critical state is reached, the band will undergo an increment of continued straining and void growth unaccompanied by additional straining at infinity. This is the onset of localization, and we will denote the remote axial strain associated with attainment of (43) by $(\varepsilon_z^\infty)_{cr}$. Depending on the details of the initial void distribution in the band, the localization process in the band may proceed to final rupture with elastic unloading occurring outside the band, or, after a certain amount of void growth in the band, the localization process may arrest such that further remote straining becomes possible. Behavior in the band subsequent to attainment of the critical state (43) will be discussed in the next section.

The corresponding critical condition is reached in the uniform infinite band problem when $L_{33}^b = 0$. From (20) it can be seen that this condition permits a strain-rate in the band with $\dot{\varepsilon}_z^b > 0$, $\dot{\varepsilon}_r^b = \dot{\varepsilon}_\theta^b = 0$, and $\dot{n}_z^b = 0$. This is the eigenstate condition for the uniform infinite band problem at which unloading outside the band begins. In the present problem for the non-uniform band, L_{33}^b becomes negative over part of the cluster region before the overall critical eigenstate characterized by (43) is reached.

4. RESULTS AND DISCUSSION

The numerical method used to solve the integral equation and the associated equations is described in the Appendix. In all cases, the remote stresses were increased proportionally with $\rho = \sigma_r^\infty/\sigma_z^\infty$ held constant. The problem is inherently incremental, and the incremental step size was adjusted to ensure small increases of strain and void volume fraction in the region in which deformation was increasing most rapidly, usually at the center ($r = 0$) of the band. In all the numerical results reported below $\nu = 0.3$, $\varepsilon_y = 0.0033$ and $N = 0.1$, except for some results on the effect of strain hardening where N is varied.

4.1. *Evolution of void distribution and critical strain*

The overall strain $(\varepsilon_z^\infty)_{cr}$ at which condition (43) for the onset of localization is met is plotted in Fig. 3 as a function of the size s of the cluster for four levels of ρ. In this figure the background initial void volume fraction is $f_1 = 0.01$ and the excess at the center of the cluster is $\Delta = 0.01$. On the left hand side of the figure a broken line indicates the bifurcation strain for an initially uniform infinite block with $f_1 = 0.01$, except for the case with $\rho = 0$ where no bifurcation occurs and the line corresponds to the limit when $\sigma_z \to 0$ ($f \to 2/3$). The dashed line on the right corresponds to the localization strain predicted by the uniform infinite band model with $f_1^b = f_1 + \Delta = 0.02$.

The model reveals that the transition between these two extreme results is a strong function of the remote triaxiality ρ. Let s_{tr} denote the value of s associated with the critical strain which falls half way between the two extreme values on the log scale of Fig. 3 (indicated by a dot in that figure). This transition value, s_{tr}, is plotted against ρ in Fig. 4. Recalling that $s\lambda$ is the approximate radius of the initial cluster, we note that the

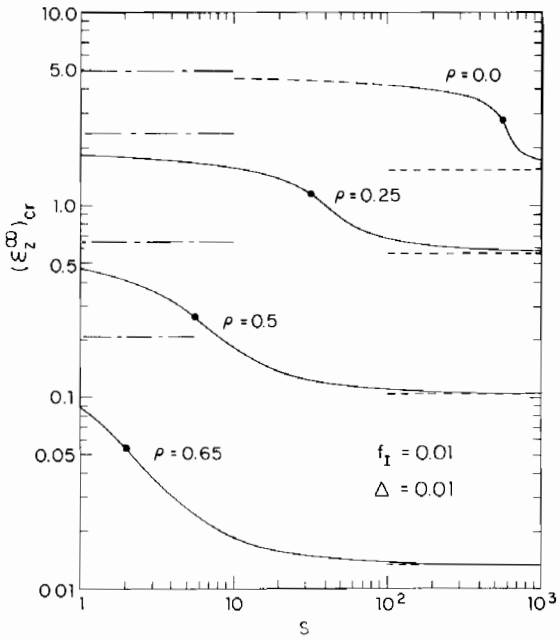

FIG 3. Ductility as a function of the measure of the size of the void cluster s for various levels of stress triaxiality ρ. In each case, $f_I = 0.01$, $\Delta = 0.01$, $\nu = 0.3$, $\varepsilon_y = 0.0033$ and $N = 0.1$. Broken lines on left indicate critical bifurcation strains for body with a uniform initial distribution of voids f_I, while dashed lines on right give localization strains based on uniform band calculations with $f_I = 0.01$ and $f_I^b - f_I = 0.01$.

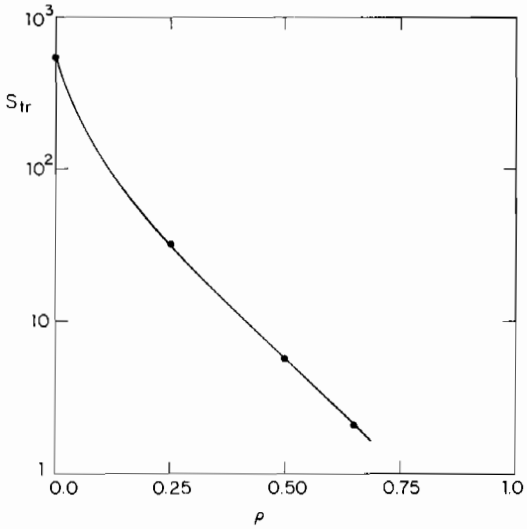

FIG. 4. Transition size of cluster as a function of the stress triaxiality level.

transition towards the uniform infinite band results occurs for a cluster radius of only about 5 void spacings when $\rho = 0.5$ and about 2 void spacings when $\rho = 0.65$, assuming λ is identified with the initial void spacing. These are high triaxiality levels but, nevertheless, characteristic of situations where plastic flow occurs under highly constrained conditions such as at the tip of a plane strain crack. The triaxiality level $\rho = 0.25$ is not untypical of values at the necked down section of a rounded tensile bar just prior to localization. At this ρ-level, a fairly large cluster of about 20 to 30 void spacings in radius is necessary to reduce the localization strain significantly below the critical strain associated with bifurcation in a block with an initially uniform distribution f_I.

Figures 5(a, b) show the evolution of void volume fraction within the band when

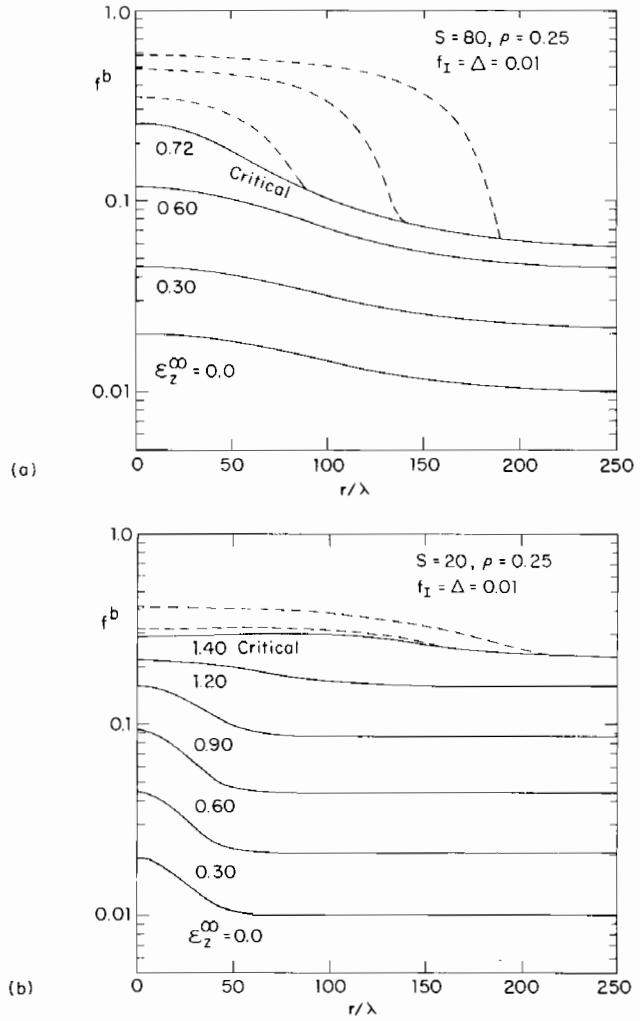

FIG. 5. Evolution of void volume fraction within the band. Dashed lines indicate evolution after critical state is attained. (a) $s = 80$. (b) $s = 20$.

$\rho = 0.25$, in (a) for a fairly large cluster ($s = 80$) and in (b) for a relatively small one ($s = 20$). For the larger cluster the voids at the center of the cluster grow much faster than those far removed from the center, so that at the localization strain $(\varepsilon_z^\infty)_{cr} = 0.72$, $f^b(0)$ is more than 4 times $f^b(\infty)$. By contrast, the peak in the initial distribution is leveled as straining proceeds in the case of the smaller cluster in Fig. 5(b). Thus in this latter case the critical strain is not much reduced below the bifurcation strain. The dashed line curves above that for the critical strain correspond to the post-critical evolution of the void volume fraction within the band which will be discussed in the next subsection.

We now ask how the larger cluster of Fig. 5(a) is able to cause localization at a strain level considerably below that required for localization in its absence. As straining proceeds the voids within the cluster grow fastest, as seen in Fig. 5(a), resulting in an increasing difference between deformation of material in the band and that outside it. As this difference becomes accentuated the *local* triaxiality level, $\sigma_{kk}/(3\sigma_e)$, in the cluster rises significantly because the band material is constrained in the radial and circumferential directions by the material outside the band which is straining more slowly. In fact when localization sets in, so that deformation outside the band ceases, the radial and circumferential strain-rates in the band become zero. The distribution of the triaxiality in the band, as measured by $\sigma_{kk}/(3\sigma_e)$, is shown in Fig. 6 for four different overall strain levels, including that at the critical state. An elevation of the local triaxiality of almost a factor of three is seen to occur near the edge of the cluster at $r = 50\lambda$. Void growth is strongly enhanced by stress triaxiality (McClintock, 1968; Rice and Tracey, 1969), and the Gurson model reflects this through the second term in the yield function (3). This strong triaxiality dependence, coupled with the tendency for triaxiality to develop as localization progresses, leads to greatly reduced overall ductility when the cluster is large enough.

Figures 7 and 8 show the effect of varying f_I and Δ on the critical strain in each case with $\rho = 0.25$. The size of the cluster associated with transition between high and low ductility is relatively insensitive to f_I and Δ; it depends mainly on ρ as previously discussed. The effect on $(\varepsilon_z^\infty)_{cr}$ of varying the strain hardening exponent N is shown in

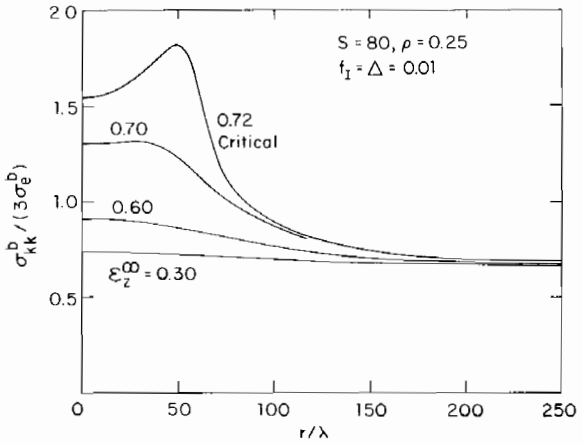

Fig. 6. Evolution of ratio of mean stress to effective stress within the band.

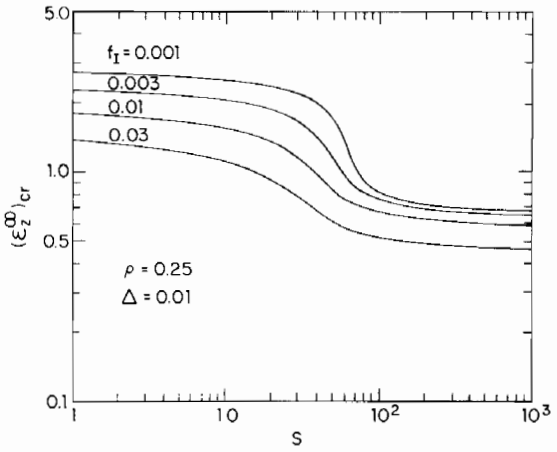

FIG. 7. Effect of f_I on ductility for constant Δ with $\rho = 0.25$.

Fig. 9. Here there is a tendency for the transition size of the cluster to decrease with increasing hardening.

4.2. *Growth of void distribution after critical state*

The critical condition (43) for the onset of localization corresponds to the attainment of an overall strain level such that an increment of strain and void growth in the band occurs with no associated increment in remote strain. Examples of the evolution of the void volume fraction distribution subsequent to attainment of the critical state are shown as dashed line curves in Figs. 5(a, b). The growth in the band beyond the critical state takes place with elastic unloading at infinity, although only a very slight drop in

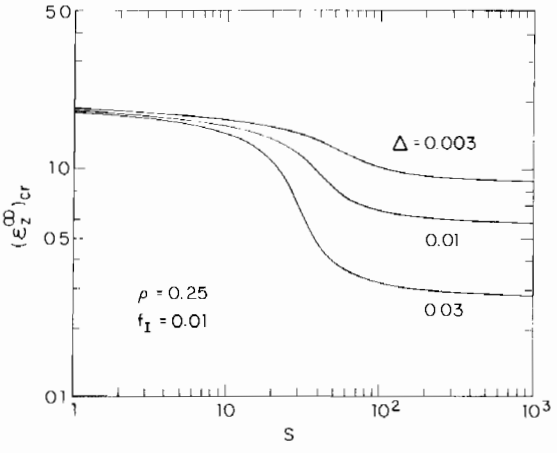

FIG. 8. Effect of Δ on ductility for constant f_I with $\rho = 0.25$.

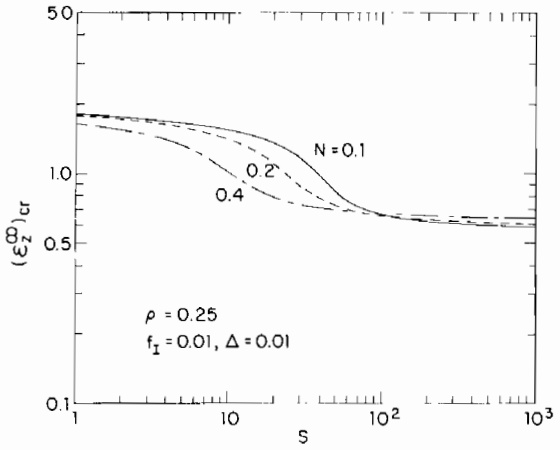

FIG. 9. Effect of strain hardening exponent N on ductility for constant f_I and Δ with $\rho = 0.25$.

the remote stress occurs. To model the post-critical incremental behavior of the material outside the band, we took

$$\dot{n}_{ij}^{\infty} = c_{ijkl}^{e}\dot{\varepsilon}_{kl}^{\infty}, \tag{44}$$

where $\mathbf{c}^e$ denotes the elastic moduli, consistent with elastic unloading at infinity. For the additional rate-quantities, which are largest near the cluster and vanish at infinity, we took

$$\dot{n}_{ij}^{*} = c_{ijkl}^{\infty}\dot{\varepsilon}_{kl}^{*}, \tag{45}$$

where $\mathbf{c}^\infty$ is the tensor of plastic loading moduli of the outer material at the critical state. Within the framework of the present model, this manner of splitting up the response for the region outside the band models in a crude way elastic unloading remote from the cluster and continued plastic load in the vicinity of the cluster. The integral equation (41) still applies with this modification if $\mathbf{L}^\infty$ is replaced by $\mathbf{L}^e$ in the expression for $\dot{q}(r)$, with the other dependencies on $\mathbf{L}^\infty$ being unaltered. In the band, the constitutive relation (18) is used exactly allowing for either plastic loading or elastic unloading.

In each case investigated in this paper the voids continue to grow in the band at essentially constant remote strain and stress once $(\varepsilon_z^\infty)_{cr}$ is attained. Figure 10 illustrates further details of the post-critical expansion of the region of localized flow for the case shown in Fig. 5(a). Figure 10(a) shows plots of the radial variation in the band of the local triaxiality level together with f and $\dot{f}/(\dot{f})_{max}$ just following attainment of the critical state. The same quantities are plotted in Fig. 10(b) after the localized region has expanded to a radius almost two times the initial cluster radius. By this stage, the highest triaxiality has developed at the outer edge of the region of localized flow and associated with this high triaxiality is a high void growth-rate. Void growth in the center of the region sheds load to the outer edge and in this way the process is self-sustaining. Note that the material in the band outside the region of localization has undergone elastic unloading. But as the region of localized flow spreads outward,

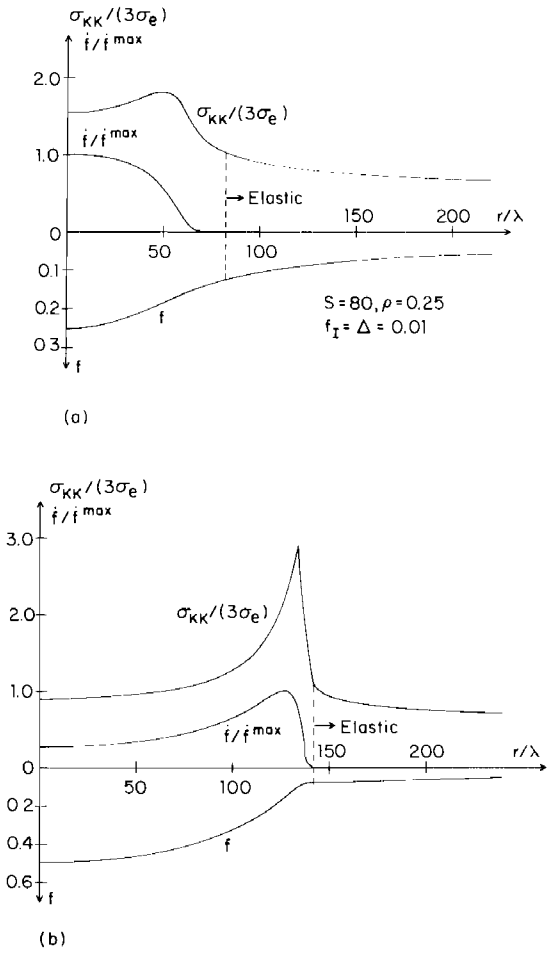

FIG. 10. Variations within the band for case $s = 80$, $\rho = 0.25$, $\Delta = 0.01$ and $f_I = 0.01$. (a) Immediately after attainment of critical state. (b) After cluster has undergone about a factor of two increase in radius by self-sustained growth.

material on the edge of this region reloads and becomes part of the expanding disk of localized flow.

Whether the process is self-sustaining or whether it arrests requiring additional remote straining to start it up again depends on the initial distribution of voids in the band. For example, if the remote initial void volume fraction f_I is zero the process will obviously arrest when the edge of the expanding localized region encounters the very low remote void levels.

4.3. *An alternative condition for the onset of localization*

TVERGAARD (1982b) has argued that the Gurson model is invalid for void volume fraction above some value f_c in the range 0.1 to 0.2. He suggests that the actual stress

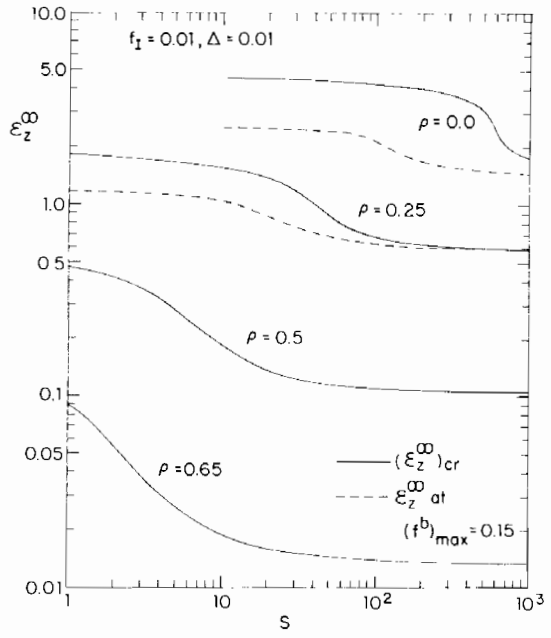

FIG. 11. Effect of alternative condition for onset of localization based on attaining a critical value of f^b.

carried by the material drops dramatically with little additional straining once f reaches f_c. Tvergaard modifies the Gurson model to reflect the sharp drop-off in stress carrying capacity for $f > f_c$.

To obtain some feeling for the sensitivity of our predictions to the details of the Gurson model, we will now say that localization starts either when the maximum value of f^b first reaches $f_c = 0.15$ or when the critical condition (43) is attained, whichever occurs first. The plot of $(\varepsilon_z^\infty)_{cr}$ based on this modified condition is shown in Fig. 11 for precisely the same parameters for the initial void distribution as was used in connection with Fig. 3. The curves from Fig. 3 are shown as solid line curves in Fig. 11, while portions of the curves for which the condition $(f)_{max} = f_c$ occurs prior to condition (43) are dashed. The results at high triaxialities are unaffected since the localization condition (43) is attained before the level f_c is reached anywhere in the cluster. At lower triaxialities the critical void level f_c is reached first. Nevertheless, the general trend of the curve of $(\varepsilon_z^\infty)_{cr}$ vs s is still the same and the transition cluster size is essentially unchanged.

5. CONCLUDING REMARKS

The present model gives further information on the sensitivity of ductility to non-uniform void distributions. The main conclusion, summarized by the results of Fig. 4, is that the smallest size of disk-shaped cluster of voids which results in a substantial reduction in ductility is a strong function of stress triaxiality. At low triaxialities, the

initial cluster must have a radius of many void spacings if it is to have a deleterious effect. At high stress triaxialities, a very small disk-like cluster can set off early localization and cause a large drop in ductility.

Any conclusions based on the model must be tempered by the fact that it is idealized in a number of respects. The Gurson theory itself, on which the model is based, is simplified representation of the behavior of voided material. Although the Gurson theory is a continuum representation, we have argued that there is some justification to regard it as characterizing each discrete cell containing one void, so that its use to describe the behavior of band material of one void spacing in thickness is not inappropriate. To simplify the analysis, the incremental properties of the material outside the band were rendered uniform and equal to those of the remote state. This approximation undoubtedly results in overly stiff material near the cluster where the higher stress levels would induce relatively lower incremental moduli. Nevertheless, this approximation may not be too significant judging from its success in an analogous study of shear localization by ABEYARATNE and TRIANTAFYLLIDIS (1981) and in certain nonlinear crack problems solved by HE and HUTCHINSON (1981) and ABEYARATNE (1983). We have neglected shearing in the band and rotation of the interface between the band and the outer material. These approximations break down when the gradients in the radial direction in the band become large, as they do when s is as small as unity. We cannot expect the result for the smallest clusters at high stress triaxiality to be very reliable. The important point, however, is that the model unambiguously indicates that small clusters are not deleterious at low triaxialities but are so at high triaxialities.

To simplify the analysis, we have restricted attention to bands orientated perpendicularly to the direction of maximum principal strain. Band orientations oblique to this direction are expected to be more critical, especially in the range of low triaxialities, and an extension of the model to deal with this more complicated situation would be of some interest.

ACKNOWLEDGEMENTS

This work was supported in part by the National Science Foundation under Grant MEA-82-13925, and by the Division of Applied Sciences, Harvard University. During the course of the work N. Ohno was a Visiting Scholar at Harvard University. Support for this stay from Toyohashi University of Technology and the Toshiba Corporation are gratefully acknowledged.

REFERENCES

ABEYARATNE, R. and TRIANTAFYLLIDIS, N. 1981 *Int. J. Solids Structures* **17**, 1113.

ABEYARATNE, R. 1983 *J. Appl. Mech.* **50**, 19.

ELLIOTT, H. A. 1948 *Proc. Camb. Phil. Soc.* **44**, 522.

ELLIOTT, H. A. 1949 *Proc. Camb. Phil. Soc.* **45**, 621.

GREEN, A. E., RIVLIN, R. S. and SHIELD, R. T. 1952 *Proc. Roy. Soc. Lond.* **A211**, 128.

GRUSON, A. L.	1975	"Plastic Flow and Fracture Behavior of Ductile Materials Incorporating Void Nucleation, Growth, and Interaction", Ph.D. Thesis, Brown University.
GURSON, A. L.	1977	*J. Engr. Materials and Technology, Trans. ASME* **99,** 2.
HE, M. Y. and HUTCHINSON, J. W.	1981	*J. Appl. Mech.* **48,** 830.
MCCLINTOCK, F. A.	1968	*J. Appl. Mech.* **35,** 363.
RICE, J. R. and TRACEY, D. M.	1969	*J. Mech. Phys. Solids* **17,** 201.
RICE, J. R.	1976	in *Theoretical and Applied Mechanics*, Proc. of the 14th IUTAM Congress, Delft (Edited by W. T. KOITER), p. 207. North Holland, Amsterdam.
SAJE, M., PAN, J. and NEEDLEMAN, A.	1982	*Int. J. Fracture* **19,** 163.
SNEDDON, I. N.	1951	*Fourier Transforms*, Chapter 2. McGraw-Hill, New York.
TVERGAARD, V.	1981	*Int. J. Fracture* **17,** 389.
TVERGAARD, V.	1982a	*Int. J. Fracture* **18,** 237.
TVERGAARD, V.	1982b	*Int. J. Solids Structures* **18,** 659.
WATSON, G. N.	1966	*A Treatise on the Theory of Bessel Functions*, 2nd Edition, Chapter 13. Cambridge University Press.
YAMAMOTO, H.	1978	*Int. J. Fracture* **14,** 347.

APPENDIX

Solution for $\dot{\mathbf{u}}^*$ *and* $\dot{\mathbf{n}}^*$ *in the semi-infinite region*

ELLIOTT (1948, 1949) obtained the general representation for the solution for a transversely isotropic elastic solid occupying the semi-infinite region $z \geqslant 0$ (see also GREEN, RIVLIN and SHIELD (1952)). The representations for $\dot{\mathbf{u}}^*$ and $\dot{\mathbf{n}}^*$ do not follow directly from this previous work since the moduli in the present problem do not possess diagonal symmetry (i.e. $c_{ijkl} \neq c_{klij}$). Nevertheless, a general representation can be obtained along similar lines, as outlined below.

First we introduce a scalar function $\phi(r, z)$ such that

$$\dot{u}_r^* = \frac{\partial \phi}{\partial r}, \qquad \dot{u}_z^* = k \frac{\partial \phi}{\partial z}, \tag{A1}$$

where k is a scalar independent of r and z. Then the equilibrium equations (28) and (29) into which (26) and (27) are substituted result in

$$L_{11}^{\infty}\left(\phi_{,rr} + \frac{1}{r}\phi_{,r}\right) + [kL_{13}^{\infty} + (1+k)L_{44}^{\infty} - \tfrac{1}{2}(1-k)\sigma_r^{\infty}]\phi_{,zz} = 0, \tag{A2}$$

$$[L_{13}^{\infty} + (1+k)L_{44}^{\infty} + \tfrac{1}{2}(1-k)\sigma_z^{\infty}]\left(\phi_{,rr} + \frac{1}{r}\phi_{,r}\right) + kL_{33}^{\infty}\phi_{,zz} = 0. \tag{A3}$$

If k is required to satisfy

$$\frac{kL_{13}^{\infty} + (1+k)L_{44}^{\infty} - (1-k)\sigma_r^{\infty}/2}{L_{11}^{\infty}} = \frac{kL_{33}^{\infty}}{L_{13}^{\infty} + (1+k)L_{44}^{\infty} + (1-k)\sigma_z^{\infty}/2} = \mu, \tag{A4}$$

(A2) and (A3) become identical to each other.

Eliminating k from (A4), we obtain

$$a\mu^2 + b\mu + c = 0, \tag{A5}$$

where

$$a = L_{11}^{\infty}(L_{44}^{\infty} - \sigma_z^{\infty}/2),$$
$$b = L_{13}^{\infty}[L_{13}^{\infty} + 2L_{44}^{\infty} + (\sigma_r^{\infty} + \sigma_z^{\infty})/2] - L_{11}^{\infty}L_{33}^{\infty} + L_{44}^{\infty}(\sigma_r^{\infty} + \sigma_z^{\infty}),$$
$$c = L_{33}^{\infty}(L_{44}^{\infty} - \sigma_r^{\infty}/2).$$

The two roots of (A5) are denoted by μ and $\bar{\mu}$.

Thus, $\dot{u}_r^*$ and $\dot{u}_z^*$ are generally expressed as

$$\dot{u}_r^* = \frac{\partial}{\partial r}(\phi + \bar{\phi}), \qquad \dot{u}_z^* = \frac{\partial}{\partial z}(k\phi + \bar{k}\bar{\phi}), \tag{A6}$$

where ϕ and $\bar{\phi}$ satisfy (A2), or (A3), for μ and $\bar{\mu}$:

$$\left.\begin{aligned} \left(\frac{\partial^2}{\partial r^2} + \frac{1}{r}\frac{\partial}{\partial r}\right)\phi + \mu\frac{\partial^2\phi}{\partial z^2} = 0, \\ \left(\frac{\partial^2}{\partial r^2} + \frac{1}{r}\frac{\partial}{\partial r}\right)\bar{\phi} + \bar{\mu}\frac{\partial^2\bar{\phi}}{\partial z^2} = 0, \end{aligned}\right\} \tag{A7}$$

and k, $\bar{k}$ are related to μ and $\bar{\mu}$, respectively, by (A4):

$$k = \frac{\mu L_{11}^{\infty} - L_{44}^{\infty} + \sigma_r^{\infty}/2}{L_{13}^{\infty} + L_{44}^{\infty} + \sigma_r^{\infty}/2}, \qquad \bar{k} = \frac{\bar{\mu} L_{11}^{\infty} - L_{44}^{\infty} + \sigma_r^{\infty}/2}{L_{13}^{\infty} + L_{44}^{\infty} + \sigma_r^{\infty}/2}. \tag{A8}$$

The components of $\dot{n}_{ij}^*$ are obtained by substituting (A6) into (26) and (27), with the result

$$\left.\begin{aligned} \dot{n}_z^* &= (L_{13}^{\infty} + \sigma_z^{\infty})\left(\frac{\partial^2}{\partial r^2} + \frac{1}{r}\frac{\partial}{\partial r}\right)(\phi + \bar{\phi}) + L_{33}^{\infty}\frac{\partial^2}{\partial z^2}(k\phi + \bar{k}\bar{\phi}), \\ \dot{n}_{zr}^* &= (L_{44}^{\infty} - \tfrac{1}{2}\sigma_r^{\infty})\frac{\partial^2}{\partial r\,\partial z}\{(1+k)\phi + (1+\bar{k})\bar{\phi}\}. \end{aligned}\right\} \tag{A9}$$

Using the zeroth-order Hankel transform with respect to r, we can obtain $\phi(r, z)$ and $\bar{\phi}(r, z)$ which satisfy (A7) (see ELLIOTT, 1949). The result is

$$\left.\begin{aligned} \phi(r, z) &= \int_0^{\infty} \xi g(\xi) \exp\left(\frac{-\xi z}{\mu^{1/2}}\right) J_0(\xi r)\,\mathrm{d}\xi, \\ \bar{\phi}(r, z) &= \int_0^{\infty} \xi \bar{g}(\xi) \exp\left(\frac{-\xi z}{\bar{\mu}^{1/2}}\right) J_0(\xi r)\,\mathrm{d}\xi. \end{aligned}\right\} \tag{A10}$$

Then, (A6) and (A9) become

$$\left.\begin{aligned} \dot{u}_r^* &= -\int_0^{\infty} \{G(\xi, z) + \bar{G}(\xi, z)\}\xi^2 J_1(\xi r)\,\mathrm{d}\xi, \\ \dot{u}_z^* &= -\int_0^{\infty} \left\{\frac{k}{\mu^{1/2}} G(\xi, z) + \frac{\bar{k}}{\bar{\mu}^{1/2}} \bar{G}(\xi, z)\right\}\xi^2 J_0(\xi r)\,\mathrm{d}\xi, \end{aligned}\right\} \tag{A11}$$

$$\left.\begin{aligned} \dot{n}_z^* &= \int_0^{\infty} \left\{\left(\frac{k}{\mu} L_{33}^{\infty} - L_{13}^{\infty} - \sigma_z^{\infty}\right) G(\xi, z) + \left(\frac{\bar{k}}{\bar{\mu}} L_{33}^{\infty} - L_{13}^{\infty} - \sigma_z^{\infty}\right)\bar{G}(\xi, z)\right\}\xi^3 J_0(\xi r)\,\mathrm{d}\xi, \\ \dot{n}_{zr}^* &= (L_{44}^{\infty} - \tfrac{1}{2}\sigma_r^{\infty}) \int_0^{\infty} \left\{\frac{1+k}{\mu^{1/2}} G(\xi, z) + \frac{1+\bar{k}}{\bar{\mu}^{1/2}} \bar{G}(\xi, z)\right\}\xi^3 J_1(\xi r)\,\mathrm{d}\xi, \end{aligned}\right\} \tag{A12}$$

where

$$G(\xi, z) = g(\xi)\exp\left(\frac{-\xi z}{\mu^{1/2}}\right), \qquad \bar{G}(\xi, z) = \bar{g}(\xi)\exp\left(\frac{-\xi z}{\bar{\mu}^{1/2}}\right).$$

Numerical method to solve integral equation (41)

We approximate $g(\xi)$ so that $\dot{n}_z^*(r,0)$ has the step-wise variation

$$n_z^*(r,0) = \sum_{j=0}^{M} \dot{p}_j[H(r_{j+1}-r)-H(r_j-r)], \tag{A13}$$

where $H(x)$ denotes the Heaviside step function, and $r_0 = 0 < r_1 < \ldots < r_{M+1}$. We now make use of the Hankel inversion theorem (see SNEDDON, 1951): When $\bar{f}^n(\xi)$ is the nth-order Hankel transform of a function $f(x)$, the reciprocal formulas are

$$f(x) = \int_0^\infty \xi \bar{f}^n(\xi) J_n(x\xi)\,\mathrm{d}\xi,$$

$$\bar{f}^n(\xi) = \int_0^\infty x f(x) J_n(\xi x)\,\mathrm{d}x.$$

Application of this theorem to (39) together with (A13) gives

$$\begin{aligned}\alpha_3 g(\xi)\xi^2 &= \sum_{j=0}^{M} \dot{p}_j \int_0^\infty r[H(r_{j+1}-r)-H(r_j-r)]J_0(\xi r)\,\mathrm{d}r \\ &= \xi^{-1} \sum_{j=0}^{M} \dot{p}_j[r_{j+1}J_1(r_{j+1}\xi)-r_jJ_1(r_j\xi)].\end{aligned} \tag{A14}$$

Substituting (A14) into the integral equation (41) and evaluating this equation at $\bar{r}_i = (r_i+r_{i+1})/2$ $(i = 0, 1, \ldots, M)$, we obtain

$$\sum_{j=0}^{M} A_{ij}\dot{p}_j = \dot{q}(\bar{r}_i), \tag{A15}$$

where

$$\begin{aligned}A_{ij} = &\left\{1 + \frac{\alpha_1}{\alpha_3}[L_{13}^{\mathrm{b}}(\bar{r}_i)+\sigma_z^{\mathrm{b}}(\bar{r}_i)]\right\}\delta_{ij} \\ &- \frac{\alpha_1}{\alpha_3}[L_{13}^{\mathrm{b}}(\bar{r}_i)-L_{23}^{\mathrm{b}}(\bar{r}_i)]\frac{1}{\bar{r}_i}[r_{j+1}U(r_{j+1},\bar{r}_i)-r_jU(r_j,\bar{r}_i)] \\ &+ \frac{\alpha_2}{\alpha_3}\frac{2L_{33}^{\mathrm{b}}(\bar{r}_i)}{\lambda \exp[\varepsilon_z^{\mathrm{b}}(\bar{r}_i)]}[r_{j+1}V(r_{j+1},\bar{r}_i)-r_jV(r_j,\bar{r}_i)],\end{aligned} \tag{A16}$$

$$U(a,r) = \int_0^\infty \xi^{-1}J_1(a\xi)J_1(r\xi)\,\mathrm{d}\xi, \tag{A17}$$

$$V(a,r) = \int_0^\infty \xi^{-1}J_1(a\xi)J_0(r\xi)\,\mathrm{d}\xi. \tag{A18}$$

Then, the critical condition (43) for plastic flow localization reduces to

$$\det A_{ij} = 0. \tag{A19}$$

Use of (A14), (37) and (38) gives

$$\dot{u}_r^*(r,0) = -\frac{\alpha_1}{\alpha_3}\sum_{j=0}^{M}[r_{j+1}U(r_{j+1},r)-r_jU(r_j,r)]\dot{p}_j, \tag{A20}$$

$$\dot{u}_z^*(r,0) = -\frac{\alpha_2}{\alpha_3}\sum_{j=0}^{M}[r_{j+1}V(r_{j+1},r)-r_jV(r_j,r)]\dot{p}_j. \tag{A21}$$

The integrals (A17) and (A18) are calculated as (see WATSON, 1966)

$$U(a,r)=\begin{cases} r/(2a), & a \geqslant r, \\ a/(2r), & r \geqslant a, \end{cases} \tag{A22}$$

$$V(a,r)=\begin{cases} F(1/2,-1/2;1;r^2/a^2), & a>r, \\ 2/\pi, & a=r, \\ (a/(2r))F(1/2,1/2;2;a^2/r^2), & r>a. \end{cases} \tag{A23}$$

Here, $F(\alpha,\beta;\gamma;z)$ denotes the hypergeometric function

$$F(\alpha,\beta;\gamma;z)=\sum_{n=0}^{\infty}\frac{(\alpha)_n(\beta)_n}{(\gamma)_n}\frac{z^n}{n!}, \tag{A24}$$

where $(\alpha)_n=\alpha(\alpha+1)(\alpha+2),\ldots,(\alpha+n-1)$, $(\alpha)_0=1$. In the case of (A23), $F(\alpha,\beta;\gamma;z)$ converges when $|z|\leqslant 1$, and $F(\alpha,\beta;\gamma;1)=\Gamma(\gamma)\Gamma(\gamma-\alpha-\beta)/\{\Gamma(\gamma-\alpha)\Gamma(\gamma-\beta)\}$ so that $V(a,r)$ is continuous at $a=r$.

When $\mathbf{L}^\infty$ and $\boldsymbol{\sigma}^\infty$ are given, α_1/α_3 and α_2/α_3 in (A16) are calculated from (A5), (A8) and (40). Therefore, if $\mathbf{L}^b(\bar{r}_i)$ $\boldsymbol{\sigma}^b(\bar{r}_i)$ are currently known too, then A_{ij} and $\dot{q}(\bar{r}_i)$ are known and one can solve for the $\mathrm{d}p_j$ in terms of $\mathrm{d}\boldsymbol{\varepsilon}^\infty$ using (A15). Then $\mathrm{d}\boldsymbol{\varepsilon}^b(\bar{r}_i)$ is obtained from (32) and (33) together with (A20) and (A21). In turn, (20) is used with (16) to determine $\mathrm{d}\boldsymbol{\sigma}^b(\bar{r}_i)$. Furthermore, $\mathrm{d}f^b(\bar{r}_i)$ and $\mathrm{d}\bar{\sigma}^b(\bar{r}_i)$ are calculated from (4) and (5). Thus, $\mathbf{L}^b(\bar{r}_i)$ and $\boldsymbol{\sigma}^b(\bar{r}_i)$ at the next step are obtained by adding those increments to the current values of the corresponding quantities. The coordinates of r_i $(i=1,2,\ldots,M+1)$ are also changed according to

$$r_i+\mathrm{d}u_r^b(r_i)=r_i+r_i\,\mathrm{d}\varepsilon_\theta^\infty+\mathrm{d}u_r^*(r_i,0), \tag{A25}$$

where $\mathrm{d}\varepsilon_\theta^\infty=\mathrm{d}\varepsilon_r^\infty$ and $\mathrm{d}u_r^*(r_i,0)$ is given by (A20).

The incremental analysis is started with the uniform stress state $\boldsymbol{\sigma}^b(r)=\boldsymbol{\sigma}^\infty$ in which the element with the largest initial void volume fraction is subject to plastic yielding, and subsequently ε_z^∞ is increased under conditions of $\rho=\sigma_r^\infty/\sigma_z^\infty=$ constant and $\sigma_r^\infty=\sigma_\theta^\infty$. In the course of the numerical analysis, the change of the sign of $\det A_{ij}$ signifies attainment of the critical state.

Before plastic yielding occurs at infinity, $\mathbf{L}^e$ is used for $\mathbf{L}^\infty$. Then, (A5) gives as the roots μ and $\bar{\mu}$ two distinct real numbers close to one. (In small strain theory when $\boldsymbol{\sigma}^\infty$ is neglected in the coefficients in (A5), $\mu=\bar{\mu}=1$.) On the other hand, when the material at infinity yields plastically, μ and $\bar{\mu}$ become complex conjugates of one another. Consequently, k and $\bar{k}$, $g(\xi)$ and $\bar{g}(\xi)$, etc. appearing are also complex conjugates of one another, and moreover α_1, α_2 and α_3 defined by (40) are complex. However, α_1/α_3 and α_2/α_3 in (A16) do take real values, since $\alpha_1 g(\xi)$, $\alpha_2 g(\xi)$ and $\alpha_3 g(\xi)$ are real, as seen in (37)–(39). In this case, additionally, care must be taken in the calculation of $\mu^{1/2}$ and $\bar{\mu}^{1/2}$ since their real parts should be positive so that $\dot{u}_i^*$ and $\dot{n}_{ij}^*$ vanish at infinity—see (A11) and (A12).

TABLE 1. *Mesh of the band for calculating critical strain* ($M+1=34, 30, 25$ *and* 25 *when* $\rho=0.0, 0.25, 0.5$ *and* 0.65, *respectively*)

i	0	1	2	3	...	13	14	15
$r_i/(\lambda s)$	0.0	0.1	0.3	0.5	...	2.5	3.0	3.5

i	...	18	19	20	21	22	$23,\ldots,M+1$
$r_i/(\lambda s)$	...	5.0	6.0	8.0	12.0	20.0	$20.0\times 2^{(i-22)}$

TABLE 2. *Influence of the sizes of loading step and mesh on* $(\varepsilon_z^\infty)_{cr}$ ($\nu = 0.3$, $\sigma_y/E = 0.0033$, $N = 0.1$, $\rho = 0.25, f_1 = \Delta = 0.01$)

s	Basic	Half load step size	Half mesh size
1.0	1.811	1.801	1.809
20.0	1.401	1.395	1.407
80.0	0.715	0.711	0.716

The analysis was performed by nondimensionalizing lengths and stresses in terms of the average void spacing length λ and Young's modulus E, respectively. Table 1 shows the mesh of the band used to calculate the critical strain. The larger the region of non-uniform deformation in the band, the larger must be M.

At each step, (A15) was solved first by taking $d\varepsilon_z^\infty = 1.0$ ($d\varepsilon_z^\infty = -1.0$ after the critical state), and then all increments added to the corresponding current values were multiplied by a loading step factor so as to satisfy the conditions $|d\sigma_i^b|_{max}/\sigma_y < 0.02$ ($i = r, \theta, z$), $(df^b)_{max} < 0.005$ and $(d\varepsilon_z^b)_{max} < \delta$, where the suffix max denotes the maximum with respect to $\bar{r}_i$ ($i = 0, 1, \ldots, M$) and $\delta = 0.01, 0.005, 0.002, 0.0002$ for $\rho = 0.0, 0.25, 0.5$, and 0.65, respectively. In addition, prior to plastic yielding at infinity, the loading step factor was specified by $(d\sigma_z^b)_{max}/\sigma_y < 0.005$. Table 2 shows the accuracy of calculation for one particular case when $\rho = 0.25$. As discussed in Section 4.2, the evolution of void-clustering after the critical state was calculated in two cases; $s = 80$ and 20 under conditions of $\rho = 0.25, f_1 = \Delta = 0.01$ and $N = 0.1$. Several initial attempts at these calculations were not successful because the mesh was not sufficiently refined to reproduce the detail at the edge of the growing cluster as seen for example in Fig. 10(b). Only when a very refined mesh was used did the calculation proceed smoothly.